NIH Public Access
Author Manuscript
Neuroimage. Author manuscript; available in PMC 2009 May 1.

Published in final edited form as:
Neuroimage. 2008 May 1; 40(4): 1595–1605.

Mapping resting-state functional connectivity using perfusion MRI

Kai-Hsiang Chuang[1], **Peter van Gelderen**[1], **Hellmut Merkle**[1], **Jerzy Bodurka**[2], **Vasiliki N. Ikonomidou**[1], **Alan P. Koretsky**[1], **Jeff H. Duyn**[1], and **S. Lalith Talagala**[3,*]

1*Laboratory of Functional and Molecular Imaging, National Institute of Neurological Disorders and Stroke, National Institutes of Health, Bethesda, MD, USA*

2*Functional MRI Facility, National Institute of Mental Health, National Institutes of Health, Bethesda, MD, USA*

3*NIH MRI Research Facility, National Institute of Neurological Disorders and Stroke, National Institutes of Health, Bethesda, MD, USA*

Abstract

Resting-state, low frequency (< 0.08 Hz) fluctuations of blood oxygenation level dependent (BOLD) magnetic resonance signal have been shown to exhibit high correlation among functionally connected regions. However, correlations of cerebral blood flow (CBF) fluctuations during the resting state have not been extensively studied. The main challenges of using arterial spin labeling perfusion magnetic resonance imaging to detect CBF fluctuations are low sensitivity, low temporal resolution, and contamination from BOLD. This work demonstrates CBF-based quantitative functional connectivity mapping by combining continuous arterial spin labeling (CASL) with a neck labeling coil and a multi-channel receiver coil to achieve high perfusion sensitivity. In order to reduce BOLD contamination, the CBF signal was extracted from the CASL signal time course by high frequency filtering. This processing strategy is compatible with sinc interpolation for reducing the timing mismatch between control and label images and has the flexibility of choosing an optimal filter cutoff frequency to minimize BOLD fluctuations. Most subjects studied showed high CBF correlation in bilateral sensorimotor areas with good suppression of BOLD contamination. Root-mean-square CBF fluctuation contributing to bilateral correlation was estimated to be 29% ± 19% (N = 13) of the baseline perfusion, while BOLD fluctuation was 0.26% ± 0.14% of the mean intensity (at 3T and 12.5 ms echo time).

Keywords

cerebral blood flow; arterial spin labeling; resting-state fluctuations; functional connectivity; sensorimotor cortex

Introduction

Blood oxygenation level dependent (BOLD) functional magnetic resonance imaging (fMRI) has been widely used to study task dependent neural activity in the brain (for reviews see Hennig et al., 2003; Matthews and Jezzard, 2004). Interestingly, even when a subject does not perform any explicit task, i.e., during the “rest” state, highly correlated small signals at low

* Correspondence to: S. Lalith Talagala, Ph.D. NIH MRI Research Facility, National Institutes of Health, 10 Center Drive, Room B1D69, Bethesda, MD 20892-1060, Email: talagala@nih.gov.

Publisher's Disclaimer: This is a PDF file of an unedited manuscript that has been accepted for publication. As a service to our customers we are providing this early version of the manuscript. The manuscript will undergo copyediting, typesetting, and review of the resulting proof before it is published in its final citable form. Please note that during the production process errors may be discovered which could affect the content, and all legal disclaimers that apply to the journal pertain.

NIH-PA Author Manuscript
NIH-PA Author Manuscript
NIH-PA Author Manuscript

NIH-PA Author Manuscript

NIH-PA Author Manuscript

NIH-PA Author Manuscript

frequency (< 0.08 Hz) can be observed in functionally connected regions such as the bilateral motor areas (Biswal et al., 1995). The correlated areas revealed by this spontaneous fluctuation are similar to those in task-dependent activation maps and have been observed in regions including sensorimotor (Biswal et al., 1995; Cordes et al., 2000; Xiong et al., 1999), visual (Cordes et al., 2000; Lowe et al., 1998), auditory (Cordes et al., 2000), language (Cordes et al., 2000; Hampson et al., 2002), and subcortical areas like thalamus (Cordes et al., 2002) and hippocampus (Rombouts et al., 2003). Moreover, large-scale, organized networks can be identified using resting-state signal fluctuations (De Luca et al., 2006; Salvador et al., 2005). It has also been suggested that correlated resting signal fluctuations among certain areas represent the “default mode” network of the brain function (Fox et al., 2005; Fransson, 2005; Greicius et al., 2003; Gusnard and Raichle, 2001; Raichle et al., 2001). Further, recent studies have demonstrated large amplitude spatially correlated BOLD signal fluctuations during extended rest and early sleep stages that are comparable to signal levels evoked by visual stimulation (Fukunaga et al., 2006b, Horovitz et al., 2007). These studies suggest that resting-state activity continues during early sleep and does not require active cognitive processes.

Functional connectivity studies using MRI have been almost exclusively performed by measuring the fluctuations in the BOLD-weighted signal. BOLD signal fluctuations represent combined changes in blood oxygenation, cerebral blood volume, cerebral blood flow (CBF) and metabolic rate of oxygen (Buxton et al., 2004). The magnitude of BOLD fluctuation is also dependent on MRI specific parameters, such as magnetic field strength and echo time (TE). In contrast, functional connectivity mapping based on CBF can provide a quantitative estimate of the fluctuations in terms of a single physiological parameter. Furthermore, similar to task activation studies, CBF based experiments may provide better localization of functionally connected regions than BOLD (Duong et al., 2001; Luh et al., 2000). Knowledge of CBF and BOLD fluctuations in the resting state will also allow the metabolic contribution to these fluctuations to be assessed (Fukunaga et al., 2006a) and oxygen consumption to be estimated as in task related functional studies (Chiarelli et al., 2007; Davis et al., 1998; Hoge et al., 1999; Kim et al., 1999).

CBF changes can be measured non-invasively by arterial spin labeling (ASL) MRI (for reviews see Barbier et al., 2001; Golay et al., 2004; Koretsky et al., 2004). The main challenges for using ASL to observe resting-state CBF fluctuations are the low sensitivity, low temporal resolution, and possible contamination from BOLD fluctuations. In ASL, perfusion sensitive MRI data is generated by inverting (labeling) the blood water magnetization in the proximal arteries prior to image acquisition. Perfusion maps are then created by subtracting ‘label’ images acquired with ASL from ‘control’ images acquired without ASL. The ASL signal in the human brain due to steady-state perfusion is on the order of 1% of the baseline MRI signal level, and the resting-state fluctuations are expected to cause only an additional fractional change. Therefore, reliable detection of changes in the perfusion signal requires high signal-to-noise ratio (SNR).

Quantitative ASL fMRI studies require acquisition of control and label images in an interleaved manner. This leads to low temporal resolution, with at least 4 – 8 s needed to acquire a single flow sensitive image. This can cause insufficient sampling of the low-frequency fluctuations. In addition, low temporal resolution also makes the perfusion images more sensitive to signal variations caused by gross head movement and physiological motion. Indeed, physiological noise due to respiratory and cardiac motion (Kruger and Glover, 2001) that are aliased to low frequency range when the image repetition time (TR) is not short enough have been suspected to contribute to the observed resting-state signal correlations (Lund, 2001). Although recent studies have shown that low-frequency signal fluctuations do not change with TR, and thus signal correlations are not caused by aliased physiological noise (Beckmann et al., 2005; Kiviniemi et al., 2005), their effects could be significant in ASL data (Restom et al., 2006).

NIH-PA Author Manuscript

NIH-PA Author Manuscript

NIH-PA Author Manuscript

Another complication is that ASL images are typically acquired using gradient-echo echo-planar imaging (EPI), which has significant T_2^*-weighting (BOLD) in each image. Since the control and label images are acquired at different times, the ASL time series is also modulated by the resting-state BOLD fluctuations. Without proper processing, signal changes due to BOLD fluctuations could be a significant confound in the pair-wise subtracted perfusion time series. Sinc interpolation can be used to correct for the timing difference between the control and label image sets and hence suppress BOLD contaminations (Aguirre et al., 2002, Liu and Wong, 2005). BOLD weighting can also be minimized by suppressing static tissue signal (Duyn et al., 2001; Ye et al., 2000). Because of timing requirements for signal nulling, this method is more appropriate when using a few 2D slices (St Lawrence et al., 2005) or single-shot 3D acquisitions. Although the use of shortest possible TE also helps to reduce BOLD related signal changes without compromising the flow sensitivity, some BOLD fluctuations will remain and contaminate the resting-state CBF signal.

To date, resting-state connectivity studies based on CBF fluctuations have been limited. The first study to demonstrate flow-weighted synchronous low-frequency signal variations used the flow alternating inversion recovery (FAIR) ASL method, and was restricted to a single slice (Biswal et al., 1997). In that work, the resting-state perfusion signal time course was generated by pair-wise subtraction of ASL time series followed by low-pass filtering. Although extraction of perfusion signal in this manner is appropriate when using very short TR, at low temporal resolution, it is not optimal and can leave a significant contribution from BOLD fluctuations. A more recent study reported detection of resting-state networks using perfusion fluctuations (De Luca et al., 2006). Although multiple slices were acquired in this study, it is not clear how the contribution from BOLD fluctuations was minimized. In another recent study, flow sensitive imaging with background suppression was employed to measure flow fluctuations during extended rest and early sleep states (Fukunaga et al., 2006a).

The purpose of this study was to develop a strategy to detect resting-state functional connectivity based on CBF with reduced contamination by BOLD effects and to characterize the CBF fluctuations responsible for connectivity between the sensorimotor areas. In this work, multi-slice flow sensitive images were acquired using continuous ASL (CASL) with a separate neck labeling coil (Garraux et al., 2005; Silva et al., 1995; Talagala et al., 2004b; Zaharchuk et al., 1999). A close fitting array receiver coil was used to provide significant gains in sensitivity (de Zwart et al., 2004; Talagala et al., 2004a; Wang et al., 2005). Some of the sensitivity gained was sacrificed to increase the temporal resolution via reduction of the labeling and post-labeling delay times. Furthermore, high-pass filtering of the ASL time course was employed to extract the CBF signal fluctuations with minimum BOLD contamination. The results show that correlated perfusion oscillations in the resting state between the sensorimotor areas can be reliably identified and quantified using CASL at 3 Tesla. Preliminary account of this work has previously appeared in abstract form (Chuang et al, 2006).

Theory

Frequency analysis of the ASL time series provides insight into how to separate the CBF and BOLD fluctuations in the resting-state data. The tissue ASL signal time course with interleaved control and label images can be formulated as

$$S(n)=M_0 \cdot [\beta - k \cdot F(n) \cdot \frac{1-\cos(\pi \cdot n)}{2}] \cdot e^{-R_2^*(n)\cdot TE}, \quad (1)$$

where n is the scan number (control and label images correspond to even and odd values of n, respectively), $F(n)$ is CBF, $R_2^*(n)$ is the effective transverse relaxation rate, TE is the echo time, and M_0 is the equilibrium magnetization. β represents the signal recovery during the

NIH-PA Author Manuscript

NIH-PA Author Manuscript

NIH-PA Author Manuscript

repetition time TR, given by $1-e^{-R_1 \cdot TR}$ where R_1 is the longitudinal relaxation rate of tissue. For CASL studies, $k=2\alpha e^{-\delta(R_{1a}-R_1)}e^{-R_1 w}\left(1-e^{-R_1\tau}\right)/\lambda R_1$ where α is the labeling efficiency, δ is the arterial blood transit time, R_{1a} is the longitudinal relaxation rate of blood, w is the post labeling delay time, τ is the labeling duration, and λ is the brain/blood partition coefficient. A similar expression for k can be derived for pulsed ASL studies.

In Eq(1), the term $e^{-R_2^*(n)\cdot TE}$ is the BOLD weighting in the image. Separating $R_2^*(n)$ into constant and time varying parts and expanding the exponential time varying term as a power series, the BOLD weighting in the image can be written as B_0 (1+ΔB(n)), where B_0 is the time invariant BOLD weighting and $\Delta B(n)$ is the fractional BOLD fluctuation. Similarly, the perfusion can be expressed as $F(n) = F_0$ (1+$\Delta F(n)$), where F_0 is the steady-state perfusion and $\Delta F(n)$ is the fractional perfusion fluctuation. Then, Eq(1) becomes:

$$S(n)=M_0\cdot[\beta-k\cdot F_0(1+\Delta F(n))\cdot\frac{1-\cos(\pi\cdot n)}{2}]\cdot B_0(1+\Delta B(n)). \quad (2)$$

The dominant fluctuating terms in Eq(2) can be identified by considering order of magnitude estimates of each term. The $\Delta B(n)$ term without perfusion, representing the resting-state BOLD fluctuation, is the largest. Typically, in a resting-state experiment, $\Delta B(n)$ will be smaller than the signal change observed in traditional task activation studies, and thus this term will be less than 1% of the baseline signal, $M_0\beta B_0$. The contribution from this term needs to be minimized in perfusion based resting-state studies. The next dominant terms involve the perfusion fluctuation, $\Delta F(n)$, which are independent of $\Delta B(n)$. $\Delta F(n)$ is expected to be on the order of several tenths of the baseline perfusion, F_0. Since the signal change due to ASL, kF_0, is ~1% of the equilibrium signal, the pure $\Delta F(n)$ terms will be about few tenths of a percent of the baseline signal and thus about a factor of 2-3 smaller than the pure BOLD term, $\Delta B(n)$. Other fluctuating terms in Eq(2) are mixtures of CBF and BOLD fluctuations. Of these, the term involving the product $kF_0\Delta B(n)$ represents the BOLD fluctuations of the steady-state perfusion signal. From the above discussion, it follows that this term and all the other CBF and BOLD interacting terms are on the order of few hundredth of a percent of the baseline signal. Since these mixed terms are much smaller than the pure CBF and BOLD fluctuations, these terms can be neglected, and Eq(2) can be approximated as

$$S(n)\approx M_0B_0[\beta-\frac{k\cdot F_0}{2}+\beta\Delta B(n)-\frac{k\cdot F_0}{2}\Delta F(n)+\frac{k\cdot F_0}{2}(1+\Delta F(n))\cos(\pi\cdot n)] \quad (3)$$

In the above equation, different terms fall into two frequency ranges. The first four terms, representing baseline signal modified by steady-state perfusion and fluctuating BOLD and perfusion components, are in the low frequency range. The last term, which represents the steady-state and fluctuating perfusion components, is modulated by the cosine term. Therefore, the contribution from this term appears in the high frequency range. Fig. 1 shows the spectra of ASL time courses simulated using Eq(2) assuming that CBF and BOLD fluctuations ($\Delta F(n)$ and $\Delta B(n)$) occur at a single (Fig. 1a) and multiple frequencies (Fig. 1b). The frequency peaks seen in Fig. 1a correspond to the pure BOLD and perfusion terms represented in Eq(3). The other mixed terms are too small to be visualized in the displayed scale. It can be seen that, while both CBF and BOLD oscillations are present in the low frequency range, only CBF components appear in the high frequency range. In practice, the fluctuations of CBF and BOLD will occur at multiple frequencies, and they will overlap in the low frequency range. As long as the frequency ranges of CBF and BOLD fluctuations are less than half of the Nyquist frequency, i.e. $\frac{1}{4TR}$, the high frequency end of the spectrum will be dominated by CBF components. Therefore, if the TR is short enough to avoid overlapping of low and high

NIH-PA Author Manuscript

NIH-PA Author Manuscript

NIH-PA Author Manuscript

frequency components (e.g. Fig. 1b), the perfusion signal can be extracted by filtering the ASL time course.

In this study, a high-pass filter was used to extract the high-frequency modulated perfusion components, and the filtered signal was demodulated to low frequency by multiplying by cos (πn). Equivalently, the ASL time course could have been demodulated and then low-pass filtered to isolate the perfusion components without BOLD effects. If the bandwidths of the fluctuating BOLD and CBF components are less than $\frac{1}{4TR}$, the cutoff frequency of the high-pass filter can be chosen as $\frac{1}{4TR}$ Hz. In the case of wider bandwidths, causing partial overlap of low and high frequency components in Eq(3), the cutoff frequency of the high-pass filter can be increased to maximally suppress the low frequency BOLD components.

The results of different methods for processing the ASL time course to isolate the perfusion signal are shown in Figs. 1c and 1d. It is seen that high-pass filtering effectively removes the undesired fluctuating BOLD component (Fig. 1c). However, at this temporal resolution (TR = 3.2s) pair-wise subtraction and low-pass filtering leaves a significant fluctuating BOLD component (Fig. 1d). The amplitude of this contaminating BOLD component is dependent on the frequency of the BOLD fluctuation relative to the sampling frequency (1/TR): being smallest at low frequencies and increasing with frequency up to the cutoff frequency of the low-pass filter. In contrast, the high-pass filtering approach (Fig. 1c) can eliminate the fluctuating BOLD components at all frequencies up to the high-pass cutoff frequency. It should be noted that high-pass filtering (Fig. 1c) with frequency cutoff at $\frac{1}{4TR}$ Hz and demodulation will produce results similar to sinc interpolation of the ASL time course to create time matched control and label images followed by subtraction (Liu and Wong, 2005).

After high-pass filtering and demodulation, the perfusion signal without BOLD contamination derived from Eq(3) is

$$S'(n) = M_0 \cdot B_0 \cdot \frac{k}{2} \cdot F_0 (1 + \Delta F(n)). \quad (4)$$

$S'(n)$ can be subjected to traditional pixel-wise correlation analysis to generate functional connectivity maps based on resting-state perfusion fluctuations, $\Delta F(n)$. It should be noted that the use of a filter to suppress BOLD fluctuations causes noise in $S'(n)$ to be reduced but correlated with the autocorrelation function determined by the characteristics of the filter. The temporal correlation of $S'(n)$ will cause correlation coefficients in the functional connectivity maps to be higher than normal. This is common to all ASL processing methods based on interpolation or filtering. Steady-state perfusion (F_0) maps, with SNR similar to that produced by pair-wise subtraction and averaging, can be created by averaging of $S'(n)$. The same processing can also be applied to perfusion-based fMRI studies with band-limited task design.

Methods

Subjects and tasks

Seventeen healthy subjects (6 males/eleven females) aged between 22 and 56 years (mean age 32 years) were recruited from the NIH database of volunteers. The research protocol was approved by the NINDS Institutional Review Board. Informed consent was obtained from all subjects. For each subject, resting-state and task activation data were collected. During the resting-state experiment, the subject was instructed to close their eyes, lie still, and keep awake without performing any specific task. This experiment lasted for about 11 min and was repeated

NIH-PA Author Manuscript

NIH-PA Author Manuscript

NIH-PA Author Manuscript

2 times: one with ASL (CBF and BOLD sensitive) and one without ASL (BOLD sensitive). Three of the subjects underwent both kinds of scans twice to evaluate the reproducibility in the same session. One subject was recruited again after 3 weeks to test the between-session reproducibility.

At the end of each scanning session, a sequential finger movement experiment was performed to localize the motor area. A block design paradigm, consisting of a 54-s rest period alternated with 54-s movement period and repeated for 5 times, was used. During the movement period, the subjects performed sequential finger-thumb opposition using the dominant hand. The movements were triggered by numbers (1-4 representing each finger) displayed on a screen at a rate of 2Hz. During the rest period, a fixation cross was displayed on the screen. The instructions were displayed on the projection screen using Presentation software (Neurobehavioral Systems, Inc., Albany, CA).

Data acquisition

Imaging was performed on a 3 Tesla whole-body MRI system (GE Healthcare, Milwaukee, WI). Studies were conducted using a 16-channel receive-only brain coil (Nova Medical, Inc., Wakefield, MA) with a custom-designed 16-channel digital receiver system (Bodurka et al., 2004; de Zwart et al., 2004) or the GE commercial 16-channel receiver system. In all cases, the body RF coil was used for excitation. The hardware used to obtain CASL data was described previously (Talagala et al., 2004b). In brief, a custom-made surface coil, consisting of two rectangular loops (6.6 cm × 4.5 cm), was placed on the neck of the subject to label the blood flowing in the right and left carotid and vertebral arteries. The labeling coil was connected to an external RF channel controlled by the scanner. The RF frequency applied to the labeling coil was offset by 16–20 kHz from center frequency according to the distance from the magnet iso-center to the labeling coil and the gradient strength (0.3 G/cm) during the labeling period. During the labeling period, the labeling coil was tuned, and the receiver coils and the body coil were detuned. During image acquisition, the labeling coil was detuned while the receiver coils and the body coil were tuned during signal reception and RF transmission, respectively.

Resting-state data were acquired under two different conditions in separate runs. First, CBF and BOLD sensitive resting-state runs were collected using CASL with interleaved control and label images. For the label images, 1.7 W of labeling RF power was applied to the neck labeling coil continuously for 2 s and followed by a 0.9-s post labeling delay and 300 ms of image acquisition. The control images were acquired by inverting the labeling gradient during the 2 s labeling period. Second, a resting-state run, sensitive only to BOLD fluctuations, was acquired by turning off the labeling RF power to the neck coil while the other experimental parameters remained the same as for the resting-state CASL runs. During the image acquisition periods in both CASL and BOLD runs, 7 axial slices with a thickness of 3 mm, a gap of 2 mm, field-of-view of 24 cm and a matrix size of 64 × 64 covering the sensorimotor area were obtained using gradient-echo EPI with TR = 3.2 s, TE = 12.5 ms, and sensitivity encoding (SENSE) acceleration factor of 2. Two hundred image volumes were collected in 10 min 40 sec.

During the finger movement task, CASL data were acquired with alternating control and label images. In this run, the labeling period was 3.0 s and the post labeling delay was 1.2 s. Other imaging parameters were the same as for the resting-state runs except for TR = 4.5 s.

Foam padding was used to minimize head movement. Respiratory and cardiac waveforms were monitored in all the subjects by a respiratory belt and a photoplethysmograph, respectively, of the scanner, and recorded by a PC using software developed in-house.

NIH-PA Author Manuscript

NIH-PA Author Manuscript

NIH-PA Author Manuscript

Data processing

Data processing was performed by software running on Matlab (MathWorks Inc, Natick, MA). To reduce gross head movement and to align the CASL and BOLD data, all the CASL (resting state and finger tapping) and BOLD images acquired in the same session were concatenated to form a long time series and realigned to their mean image in two passes using SPM2 (Friston KJ, 1995). Data from 4 subjects (2 males, 2 females) showed significant head movement (> 1 pixel), and hence were discarded from further analysis. Realigned data were then subjected to retrospective image-based physiological noise correction (Chuang and Chen, 2001; Glover et al., 2000) to remove signal fluctuation due to respiratory and cardiac effects. In this procedure, time-series images were reordered into a unit respiratory/cardiac cycle based on the recorded respiratory/cardiac waveforms. The trend of the signal change within the respiratory/cardiac cycle was then fitted using a 2^{nd} order Fourier series and the fitted trend was subtracted from each pixel time series. Because of the intensity differences, the control and label images in the CASL data were subjected to physiological noise correction separately (Restom et al., 2006).

Perfusion signal components in the resting-state CASL signal time course were extracted using a 5^{th} order Chebyshev type I high-pass filter with cutoff at 0.08 Hz covering the reported range of the resting-state BOLD fluctuations (Biswal et al., 1995; Lowe et al., 1998). The filtered time course was then demodulated by multiplying by $\cos(\pi n)$. CASL data processed in this manner will be referred to as “high-pass CASL”.

To evaluate the effectiveness of high-pass filtering in suppressing BOLD fluctuations, the resting-state BOLD data were also processed the same way as the resting-state CASL data. BOLD data processed in this manner will be referred to as “high-pass BOLD”. Since resting-state BOLD data are not modulated by flow sensitive spin labeling, high-pass filtering should remove all fluctuating signal components as long as BOLD fluctuations are band limited to 0.08 Hz. Therefore, high-pass BOLD data are not expected to produce any correlated areas in the functional connectivity maps. In addition, the resting-state BOLD data were also processed in the traditional way to produce BOLD-based functional connectivity maps using a high-pass filter cutoff at 0.003 Hz to remove the baseline drift. These results will be referred to as “standard BOLD”. Since the SNR was sufficiently high, no spatial smoothing was used either in CASL or BOLD data to avoid reduction in resolution.

Functional connectivity was detected by correlation analysis of resting-state data. A region of interest (ROI) in the sensorimotor area was defined as the voxels identified in the activation maps of the finger movement data (see below). The average time course within this reference ROI was correlated with the individual time courses of all the pixels in the brain. The correlation coefficient (CC) maps were thresholded at a CC = 0.4 (uncorrected $p < 0.0001$ for high-pass filtered data) or higher with a cluster size of at least 4 pixels. The p-value for high-pass filtered data, which accounted for temporal correlation, was determined using simulations. The same ROI location and the CC threshold were used for the resting state CASL and BOLD data within each subject.

The motion corrected and realigned CASL data acquired during the finger movement task were analyzed by cross-correlation of the pair-wise difference (control – label) image series with a boxcar function representing the finger movement paradigm. The resulting statistical maps were thresholded at CC = 0.3 (uncorrected $p < 0.02$) with a cluster size of 4 pixels to identify activated pixels. The average CBF change of the activated pixels in the sensorimotor area was calculated as the ratio of the difference image intensity during the task and rest periods. The control images without subtraction were also processed similarly to obtain the average BOLD signal change due to the finger movement task.

NIH-PA Author Manuscript

NIH-PA Author Manuscript

NIH-PA Author Manuscript

For quantitative comparisons, the dominant frequencies that contribute to resting-state connectivity were identified by spectral analysis of the CC (Cordes et al., 2000) between the ROI time courses in the left and right sensorimotor areas. In this analysis, the CC is expressed using the discrete inverse Fourier coefficients of the time courses and a correlation coefficient spectrum that represents the frequency specific correlation coefficient (cc_f) is derived. CC spectra from each data set (high-pass CASL, high-pass BOLD and standard BOLD) were calculated using the average time courses from the reference ROI time and the pixels in the contralateral sensorimotor cortex identified in the high-pass CASL connectivity map. The major frequencies that contribute to correlation were identified by thresholding the CC spectra at mean + 2 × standard deviation (STD) of the cc_f of the high-pass BOLD CC spectrum (frequency range 0.08-0.15 Hz). This threshold was typically between $cc_f = 0.01$ and 0.02 for different subjects. The frequencies surviving this cc_f threshold in the reference ROI time course were extracted by a frequency-domain filter and inverse Fourier transformed to time domain. The root-mean-square (RMS) amplitudes of the time domain signals, representing the integrated amplitude of the major frequencies, were calculated. The amplitudes of extracted time domain signals of high-pass CASL and high-pass BOLD data, normalized respectively by the intensities of control and original images, were compared to evaluate the level of BOLD fluctuation remaining after high-pass filtering. To estimate the CBF and BOLD fluctuation amplitudes related to functional connectivity, the extracted time domain signals from high-pass CASL and standard BOLD data were normalized by the baseline CBF and original image intensity, respectively.

The within-session reproducibility of the connectivity maps was measured by a similarity index (*SI*) given by,

$$SI = \frac{\sum (C1 \cdot C2)}{\sqrt{\sum (C1 \cdot C1) \sum (C2 \cdot C2)}} \quad (5)$$

where *C*1 and *C*2 are the un-thresholded correlation maps of the 1st and the 2nd runs, respectively, reformatted to one dimension. Equation 5 calculates the normalized inner product of two vectors which can be regarded as the spatial correlation between the two connectivity maps (van Gelderen et al., 2005). The same procedure was also applied to calculate the similarity between the BOLD and CBF connectivity maps.

Results

Typical CASL and BOLD resting-state data from a volunteer is shown in Fig. 2. Inspection of the unprocessed signal time courses from an ROI in the motor area (the green region in Fig. 2c) shows that the time course of CASL data contains a high frequency oscillation due to the intensity modulation caused by alternate acquisition of arterial spin label and control images, while the time course of BOLD data shows a slow fluctuation (Fig. 2a). This can be seen more clearly in the magnitude spectra of the time courses calculated by discrete Fourier transform. The frequency domain representations of both time courses show that the spectral energy of BOLD fluctuations is confined to the low frequency range from 0.01 to 0.04 Hz (Fig. 2b). However, in addition to the low frequencies, the high frequency range of the CASL spectrum contains a main peak at the modulating frequency, which corresponds to the steady-state CBF, and sideband frequencies around 0.14 Hz, which correspond to CBF fluctuations. Since the fluctuating components of BOLD and CBF signals are well separated in the frequency domain, BOLD contamination in the CBF signal can be suppressed by high-pass filtering of CASL data. Fig. 2c shows the functional connectivity maps created by correlating the ROI time course from the left motor area with time courses of all the pixels in the brain. The CBF fluctuations isolated with high-pass CASL data exhibit strong correlation between the left sensorimotor area and the right sensorimotor and supplementary motor areas (Fig. 2c left). As expected,

NIH-PA Author Manuscript

NIH-PA Author Manuscript

NIH-PA Author Manuscript

standard BOLD data also show bilateral correlation due to low frequency fluctuations in the BOLD weighted signal (Fig 2c, 2nd from the left). This bilateral correlation is absent in the high-pass BOLD data (Fig. 2c, 3rd from the left), while it is still present in the pair-wise subtracted and low-pass filtered BOLD data (Fig. 2c right). In agreement with the simulations (Figs. 1c and 1d), observation of residual correlations in the pair-wise subtracted BOLD data but not in high-pass BOLD data indicates that high-pass filtering is an effective approach for suppressing BOLD fluctuations in CBF-based connectivity maps.

Fig. 3 shows multi-slice functional connectivity results from another subject. The spectra of the ROI time-courses show well separated BOLD and CBF fluctuations (Fig. 3a). The functional connectivity maps show high correlation between the left and the right sensorimotor areas across several slices in the high-pass CASL (Fig. 3b top row) and standard BOLD (Fig. 3b middle row) data. No bilateral correlation is seen in the high-pass BOLD data (Fig. 3b bottom row) indicating that contribution of BOLD fluctuations in the CBF-based connectivity maps (Fig. 3b top row) is minimal.

The BOLD signal fluctuation remaining after high-pass filter processing was evaluated by comparing the time domain RMS signal amplitude of frequencies contributing to bilateral correlation in the high-frequency range (> 0.08 Hz). Fig. 4 shows the percent RMS amplitudes of high-pass CASL and high-pass BOLD data from all subjects. The RMS amplitude of the selected frequencies in high-pass CASL (0.104% ± 0.038%, mean ± STD, N = 13) is significantly higher than that in high-pass BOLD (0.061% ± 0.028%, $p < 0.001$, two-tail paired *t*-test). The RMS signal amplitude in high-pass CASL represents the fluctuation level of CBF while that in high-pass BOLD represents the residual BOLD fluctuations, along with some contribution from noise in both cases. Significantly lower RMS signal in high-pass BOLD data indicates that BOLD fluctuations can be effectively suppressed by high-pass filtering. However, one subject showed similar RMS signal amplitudes in high-pass CASL and high-pass BOLD data. This is attributed to the presence of high-frequency BOLD fluctuations that extended beyond the specified filter cutoff frequency (0.08 Hz). Inspection of BOLD spectra of this subject revealed a higher signal power in the high frequency range (0.08 – 0.15 Hz) but not discrete peaks.

CBF connectivity maps were found to be reproducible across different runs in the same session (Fig. 5). The similarity indices of within-session connectivity maps for the three subjects were 0.79, 0.88, and 0.77. Note that this index is not affected by the CC thresholds used for the images in Fig. 5 because it was calculated from unthresholded correlation maps. The between-session maps obtained in one subject examined 3 weeks apart were similar. Due to limited number of slices, the data obtained 3 weeks apart could not be reliably registered, and thus, the similarity index between the connectivity maps could not be calculated. The spectral distribution of the dominant CBF peaks was found to be very similar in both the within- and between-session tests. The within-session functional connectivity maps created from standard BOLD were also found to be highly reproducible with similarity indices of 0.81, 0.93, and 0.85 in the three subjects.

Most subjects showed reasonable agreement between CBF and BOLD connectivity maps in the sensorimotor area (Fig. 6). The similarity index between unthresholded correlation maps of CASL and BOLD data was 0.56 ± 0.11 (mean ± STD, N = 13). The overlapping region between thresholded CBF and BOLD connectivity maps in all the slices was 55% ± 20% of the area of the CBF maps.

Table 1 shows the estimated CBF and BOLD fluctuation amplitudes giving rise to correlation between left and right sensorimotor areas. The average RMS CBF fluctuation was 29% ± 19% (mean ± STD, N = 13) and the RMS BOLD fluctuation was 0.26% ± 0.14%. The RMS CBF

NIH-PA Author Manuscript

NIH-PA Author Manuscript

NIH-PA Author Manuscript

and BOLD fluctuations that include all frequency components were 51% ± 37% and 0.34% ± 0.13%, respectively. In comparison, the average signal change during the finger movement task was 73% ± 17% for CBF and 0.53% ± 0.14% for BOLD (N = 9). The peak frequencies of the CBF and BOLD fluctuations were different in all cases. The average peak frequencies of CBF and BOLD were 0.026 ± 0.018 Hz and 0.017 ± 0.008 Hz, respectively.

Discussion

In this work, we have demonstrated that resting-state functional connectivity can be reliably detected using perfusion MRI. Current results also confirm earlier reports on correlated CBF fluctuations in the bilateral sensorimotor areas (Biswal et al., 1997). High perfusion sensitivity achieved by combining multi-channel receiver coils and CASL with a separate neck labeling coil generated reproducible CBF-based functional connectivity maps across multiple slices covering the sensorimotor cortex. Furthermore, a filter-based processing strategy was shown to be effective in extracting the CBF signal from CASL time course while suppressing BOLD fluctuations. This processing method is based on the fact that perfusion signal is frequency shifted by turning the labeling on/off in the ASL image time series. Frequency domain analysis of the ASL signal time course according to the on-off labeling frequency has previously been used in dynamic ASL studies (Barbier et al., 1999). CBF-based functional connectivity in the bilateral sensorimotor areas was observed with good within-session reproducibility. The study also provided an estimate of the magnitude of dominant CBF fluctuating components in the resting state.

In most ASL imaging, perfusion information is obtained by pair-wise subtraction. While this would be appropriate for measuring steady-state perfusion, it is not suitable for dynamic studies such as perfusion-based functional connectivity mapping and fMRI. This is due to the fact that control and label ASL images, which are acquired at different times, may contain different BOLD weighting and pair-wise subtraction leaves a residual BOLD contribution that may vary with time. Subtraction with sinc interpolation has been suggested to be an optimal method for block-design ASL fMRI (Liu and Wong, 2005). Indeed, when the signal bandwidth due to task related changes is less than half of the Nyquist frequency, sinc interpolation is ideal for compensating the signal variation caused by the timing mismatch between control and label images. In block design studies this condition is easily satisfied, since several control/label image pairs are normally acquired during each experimental condition block. However, when the signal bandwidth exceeds that limit, the sampling requirement for sinc interpolation is not satisfied, and this approach can lead to erroneous results. This case may be encountered more often in resting-state and event-related experiments. Therefore, care should be taken when processing resting-state ASL data especially when the TR is not short compared to the time scale of the relevant physiological processes. In the current study, this problem was addressed by employing a filter-based processing strategy. As shown before, sinc subtraction of ASL data is equivalent to applying an ideal low-pass filter to demodulated data with filter cutoff frequency at half the Nyquist frequency (Liu and Wong, 2005). However, direct filtering of ASL time course offers the flexibility of choosing the optimal cutoff frequency and therefore, provides a more general approach to reduce BOLD contamination in resting-state ASL studies.

In this study, the efficacy of high-pass filtering in suppressing BOLD fluctuations was evaluated by acquiring another run of data with identical imaging parameters but without labeling RF power. Thus this data is only sensitive to BOLD fluctuations. High-pass filtering successfully suppressed bilateral sensorimotor correlation in these BOLD data sets. Further, the RMS signal in the high-pass BOLD data was found to be significantly lower than that of high-pass CASL data indicating that high-pass filtering is an effective approach to control BOLD contamination in perfusion based resting state studies. This method becomes less effective in subjects with strong BOLD fluctuations extending close to the Nyquist frequency,

NIH-PA Author Manuscript

NIH-PA Author Manuscript

NIH-PA Author Manuscript

which is 0.156 Hz in the current study. In general, CASL data series with higher temporal resolution (shorter TR) will provide better separation of BOLD and CBF fluctuations.

Respiration and cardiac pulsation induced signal variations are usually suspected to contribute to the observed signal correlation in the resting-state studies when the TR is not short (Bhattacharyya and Lowe, 2004; Lund, 2001). In this work we used image-based retrospective correction to reduce physiological noise (Chuang and Chen, 2001; Glover et al., 2000). However, variations in heart rate, respiratory rate and volume may still contribute to signal fluctuations. A recent study found that default-mode network became more restricted when subjects were cued to breathe at a constant rate and depth (Birn et al., 2006). BOLD signal fluctuations has also recently been found to correlate with low frequency variations of the heart rate (Shmueli et al., 2007).

Good correspondence was observed between the CBF and BOLD functional connectivity maps. BOLD maps generally showed strong interhemispheric correlation, although the TE used in this study was not optimized for BOLD contrast. The correlation between the sensorimotor area and the supplementary motor area reported in previous BOLD studies (Salvador et al., 2005; Xiong et al., 1999) and CBF studies using positron emission tomography (Young et al., 2003) was also found in some of our CBF and BOLD results.

A useful feature of CBF-based functional connectivity mapping is its quantitative nature. In the current study, spectral analysis of CC was used to identify the frequencies that contributed to the bilateral correlation, and the signal changes more related to connectivity was identified. The RMS CBF change that contributed to the bilateral motor correlation was 29% of the steady-state perfusion, and the BOLD change was 0.26% of the mean signal intensity (at TE = 12.5 ms). The corresponding amplitudes of CBF and BOLD fluctuations that included all frequency components were 51% and 0.34%, respectively. Assuming a linear increase in BOLD fluctuations with TE and a measured average steady-state perfusion signal of 1.05% of the baseline signal, the ratio of the observed BOLD to perfusion fluctuations that include all frequency components at TE = 35 ms is 1.78. This BOLD-perfusion fluctuation ratio is close to the value of 1.57 reported recently (Fukunaga et al., 2006a).

In this study, both the resting-state CBF and BOLD fluctuation amplitudes contributing to bilateral correlation in the motor area were found to be ~40% of the task activation signal. Inclusion of all the frequency components in the time course caused the RMS amplitude of resting-state CBF and BOLD fluctuation to be ~60% of the task activation. This value is, however, higher than that found in a previous study which reported that resting-state BOLD signal to be about 1/3 of the task activation without frequency discrimination (Peltier and Noll, 2002).

A limitation of the present study is the restricted brain coverage due to short image acquisition time. The reduced number of useable slices after motion correction and spatial normalization also made group analysis of data not practical. In future studies, the slice coverage in perfusion based resting state studies can be improved by using 3D acquisitions without sacrificing temporal resolution. In addition, background suppression pulses could be used with 3D imaging to further decrease BOLD contribution in CBF connectivity maps. Recent literature indicate that perfusion studies with whole-brain coverage can be obtained with reasonable resolution and imaging duration using various 3D acquisition schemes (Fernandez-Seara et al., 2005; Gunther et al., 2005; Talagala et al., 2006). Another drawback in the present study is the use of short post labeling delay times in an effort to minimize the TR. In cases where this post labeling delay may not be long enough to minimize the arterial transit time effect (Alsop and Detre, 1996), some arterial signal may have contributed to the CBF images. In future studies, a shorter labeling time and a longer post labeling delay may be used to minimize this effect

NIH-PA Author Manuscript

NIH-PA Author Manuscript

NIH-PA Author Manuscript

without significant effect on the perfusion sensitivity and temporal resolution. Bipolar gradients can also be used to dephase the signal in larger vessels (Ye et al., 1997). This approach may also allow use of shorter post labeling delays leading to higher temporal resolution.

Conclusion

This study demonstrates that correlated CBF oscillations across different brain regions can be reliably identified at 3 Tesla by combination of CASL with a neck labeling coil and parallel imaging with multi-channel receive-only brain surface coil arrays. High-pass filtering of the ASL signal allowed CBF oscillations to be isolated with reduced BOLD contamination. This processing method is consistent with sinc subtraction, but has flexibility of choosing an optimal filter cutoff frequency to minimize BOLD fluctuations. Combining these techniques with 3D imaging will allow CBF-based functional connectivity mapping throughout the brain in the future.

Acknowledgements

This research was supported by the Intramural Research Program of the NINDS, NIH.

References

Aguirre GK, Detre JA, Zarahn E, Alsop DC. Experimental design and the relative sensitivity of BOLD and perfusion fMRI. Neuroimage 2002;15:488–500. [PubMed: 11848692]

Alsop DC, Detre JA. Reduced transit-time sensitivity in noninvasive magnetic resonance imaging of human cerebral blood flow. J Cereb Blood Flow Metab 1996;16:1236–1249. [PubMed: 8898697]

Barbier EL, Lamalle L, Decorps M. Methodology of brain perfusion imaging. J Magn Reson Imaging 2001;13:496–520. [PubMed: 11276094]

Barbier EL, Silva AC, Kim HJ, Williams DS, Koretsky AP. Perfusion analysis using dynamic arterial spin labeling (DASL). Magn Reson Med 1999;41:299–308. [PubMed: 10080277]

Beckmann CF, DeLuca M, Devlin JT, Smith SM. Investigations into resting-state connectivity using independent component analysis. Philos Trans R Soc Lond B Biol Sci 2005;360:1001–1013. [PubMed: 16087444]

Bhattacharyya PK, Lowe MJ. Cardiac-induced physiologic noise in tissue is a direct observation of cardiac-induced fluctuations. Magn Reson Imaging 2004;22:9–13. [PubMed: 14972388]

Birn RM, Diamond JB, Smith MA, Bandettini PA. Separating respiratory-variation-related fluctuations from neuronal-activity-related fluctuations in fMRI. Neuroimage 2006;31:1536–1548. [PubMed: 16632379]

Biswal B, Van Kylen J, Hyde JS. Simultaneous assessment of flow and BOLD signals in resting-state functional connectivity maps. NMR Biomed 1997;10:165–170. [PubMed: 9430343]

Biswal B, Yetkin FZ, Haughton VM, Hyde JS. Functional connectivity in the motor cortex of resting human brain using echo-planar MRI. Magn Reson Med 1995;34:537–541. [PubMed: 8524021]

Bodurka J, Ledden PJ, van Gelderen P, Chu R, de Zwart JA, Morris D, Duyn JH. Scalable multichannel MRI data acquisition system. Magn Reson Med 2004;51:165–171. [PubMed: 14705057]

Buxton RB, Uludag K, Dubowitz DJ, Liu TT. Modeling the hemodynamic response to brain activation. Neuroimage 2004;23:S220–233. [PubMed: 15501093]

Chiarelli PA, Bulte DP, Gallichan D, Piechnik SK, Wise R, Jezzard P. Flow-metabolism coupling in human visual, motor, and supplementary motor areas assessed by magnetic resonance imaging. Magn Reson Med 2007;57:538–547. [PubMed: 17326178]

Chuang KH, Chen JH. IMPACT: image-based physiological artifacts estimation and correction technique for functional MRI. Magn Reson Med 2001;46:344–353. [PubMed: 11477639]

Chuang, KH.; van Gelderen, P.; Bodurka, J.; Ikonomidou, VN.; Koretsky, AP.; Duyn, JH.; Talagala, SL. Mapping resting-state functional connectivity by perfusion MRI Proc 14th Annual Meeting. ISMRM; Seattle, WA: 2006. p. 534

NIH-PA Author Manuscript

NIH-PA Author Manuscript

NIH-PA Author Manuscript

Cordes D, Haughton V, Carew JD, Arfanakis K, Maravilla K. Hierarchical clustering to measure connectivity in fMRI resting-state data. Magn Reson Imaging 2002;20:305–317. [PubMed: 12165349]

Cordes D, Haughton VM, Arfanakis K, Wendt GJ, Turski PA, Moritz CH, Quigley MA, Meyerand ME. Mapping functionally related regions of brain with functional connectivity MR imaging. AJNR Am J Neuroradiol 2000;21:1636–1644. [PubMed: 11039342]

Davis TL, Kwong KK, Weisskoff RM, Rosen BR. Calibrated functional MRI: mapping the dynamics of oxidative metabolism. Proc Natl Acad Sci U S A 1998;95:1834–1839. [PubMed: 9465103]

De Luca M, Beckmann CF, De Stefano N, Matthews PM, Smith SM. fMRI resting state networks define distinct modes of long-distance interactions in the human brain. Neuroimage 2006;29:1359–1367. [PubMed: 16260155]

de Zwart JA, Ledden PJ, van Gelderen P, Bodurka J, Chu R, Duyn JH. Signal-to-noise ratio and parallel imaging performance of a 16-channel receive-only brain coil array at 3.0 Tesla. Magn Reson Med 2004;51:22–26. [PubMed: 14705041]

Duong TQ, Kim DS, Ugurbil K, Kim SG. Localized cerebral blood flow response at submillimeter columnar resolution. Proc Natl Acad Sci U S A 2001;98:10904–10909. [PubMed: 11526212]

Duyn JH, Tan CX, van Gelderen P, Yongbi MN. High-sensitivity single-shot perfusion-weighted fMRI. Magn Reson Med 2001;46:88–94. [PubMed: 11443714]

Fernandez-Seara MA, Wang Z, Wang J, Rao HY, Guenther M, Feinberg DA, Detre JA. Continuous arterial spin labeling perfusion measurements using single shot 3D GRASE at 3 T. Magn Reson Med 2005;54:1241–1247. [PubMed: 16193469]

Fox MD, Snyder AZ, Vincent JL, Corbetta M, Van Essen DC, Raichle ME. The human brain is intrinsically organized into dynamic, anticorrelated functional networks. Proc Natl Acad Sci U S A 2005;102:9673–9678. [PubMed: 15976020]

Fransson P. Spontaneous low-frequency BOLD signal fluctuations: an fMRI investigation of the resting-state default mode of brain function hypothesis. Hum Brain Mapp 2005;26:15–29. [PubMed: 15852468]

Friston KJ, A J, Frith CD, Poline JB, Heather JD, Frackowiak RSJ. Spatial registration and normalization of images. Human Brain Mapping 1995;3:165–189.

Fukunaga, M.; Horovitz, SG.; de Zwart, JA.; van Gelderen, P.; Fulton, SC.; Balkin, TJ.; Duyn, JH. Metabolic origin of BOLD signal fluctuations during extended rest and light sleep. Proc 14th Annual Meeting ISMRM; 2006a. p. 372

Fukunaga M, Horovitz SG, van Gelderen P, de Zwart JA, Jansma JM, Ikonomidou VN, Chu R, Deckers RHR, Leopold DA, Duyn JH. Large amplitude, spatially correlated fluctuations in BOLD fMRI signals during extended rest and early sleep stages. Magn Reson Imaging 2006b;24:979–992. [PubMed: 16997067]

Garraux G, Hallett M, Talagala SL. CASL fMRI of subcortico-cortical perfusion changes during memory-guided finger sequences. Neuroimage 2005;25:122–132. [PubMed: 15734349]

Glover GH, Li TQ, Ress D. Image-based method for retrospective correction of physiological motion effects in fMRI: RETROICOR. Magn Reson Med 2000;44:162–167. [PubMed: 10893535]

Golay X, Hendrikse J, Lim TC. Perfusion imaging using arterial spin labeling. Top Magn Reson Imaging 2004;15:10–27. [PubMed: 15057170]

Greicius MD, Krasnow B, Reiss AL, Menon V. Functional connectivity in the resting brain: a network analysis of the default mode hypothesis. Proc Natl Acad Sci U S A 2003;100:253–258. [PubMed: 12506194]

Gunther M, Oshio K, Feinberg DA. Single-shot 3D imaging techniques improve arterial spin labeling perfusion measurements. Magn Reson Med 2005;54:491–498. [PubMed: 16032686]

Gusnard DA, Raichle ME. Searching for a baseline: functional imaging and the resting human brain. Nat Rev Neurosci 2001;2:685–694. [PubMed: 11584306]

Hampson M, Peterson BS, Skudlarski P, Gatenby JC, Gore JC. Detection of functional connectivity using temporal correlations in MR images. Hum Brain Mapp 2002;15:247–262. [PubMed: 11835612]

Hennig J, Speck O, Koch MA, Weiller C. Functional magnetic resonance imaging: a review of methodological aspects and clinical applications. J Magn Reson Imaging 2003;18:1–15. [PubMed: 12815634]

NIH-PA Author Manuscript

NIH-PA Author Manuscript

NIH-PA Author Manuscript

Hoge RD, Atkinson J, Gill B, Crelier GR, Marrett S, Pike GB. Investigation of BOLD signal dependence on cerebral blood flow and oxygen consumption: the deoxyhemoglobin dilution model. Magn Reson Med 1999;42:849–863. [PubMed: 10542343]

Horovitz SG, Fukunaga M, de Zwart JA, van Gelderen P, Fulton SC, Balkin TJ, Duyn JH. Low frequency BOLD fluctuations during resting wakefulness and light sleep: A simultaneous EEG-fMRI study. Hum Brain Mapp. 2007

Kim SG, Rostrup E, Larsson HB, Ogawa S, Paulson OB. Determination of relative CMRO2 from CBF and BOLD changes: significant increase of oxygen consumption rate during visual stimulation. Magn Reson Med 1999;41:1152–1161. [PubMed: 10371447]

Kiviniemi V, Ruohonen J, Tervonen O. Separation of physiological very low frequency fluctuation from aliasing by switched sampling interval fMRI scans. Magn Reson Imaging 2005;23:41–46. [PubMed: 15733787]

Koretsky, AP.; Talagala, SL.; Keilholz, SD.; Silva, AC. MRI detection of regional blood flow using arterial spin labeling. In: G, HJ.; W, DA.; B, BP., editors. Clinical MR Neuroimaging: Diffusion, Perfusion and Spectroscopy. Cambridge University Press; 2004. p. 119-140.

Kruger G, Glover GH. Physiological noise in oxygenation-sensitive magnetic resonance imaging. Magn Reson Med 2001;46:631–637. [PubMed: 11590638]

Liu TT, Wong EC. A signal processing model for arterial spin labeling functional MRI. Neuroimage 2005;24:207–215. [PubMed: 15588612]

Lowe MJ, Mock BJ, Sorenson JA. Functional connectivity in single and multislice echoplanar imaging using resting-state fluctuations. Neuroimage 1998;7:119–132. [PubMed: 9558644]

Luh WM, Wong EC, Bandettini PA, Ward BD, Hyde JS. Comparison of simultaneously measured perfusion and BOLD signal increases during brain activation with T(1)-based tissue identification. Magn Reson Med 2000;44:137–143. [PubMed: 10893532]

Lund TE. fcMRI--mapping functional connectivity or correlating cardiac-induced noise? Magn Reson Med 2001;46:628–629. [PubMed: 11550260]

Matthews PM, Jezzard P. Functional magnetic resonance imaging. J Neurol Neurosurg Psychiatry 2004;75:6–12. [PubMed: 14707297]

Peltier SJ, Noll DC. T2* dependence of low frequency functional connectivity. Neuroimage 2002;16:985–992. [PubMed: 12202086]

Raichle ME, MacLeod AM, Snyder AZ, Powers WJ, Gusnard DA, Shulman GL. A default mode of brain function. Proc Natl Acad Sci U S A 2001;98:676–682. [PubMed: 11209064]

Restom K, Behzadi Y, Liu TT. Physiological noise reduction for arterial spin labeling functional MRI. Neuroimage 2006;31:1104–1115. [PubMed: 16533609]

Rombouts SA, Stam CJ, Kuijer JP, Scheltens P, Barkhof F. Identifying confounds to increase specificity during a “no task condition”. Evidence for hippocampal connectivity using fMRI. Neuroimage 2003;20:1236–1245. [PubMed: 14568492]

Salvador R, Suckling J, Coleman MR, Pickard JD, Menon D, Bullmore E. Neurophysiological Architecture of Functional Magnetic Resonance Images of Human Brain. Cereb Cortex 2005;15:1332–1342. [PubMed: 15635061]

Shmueli K, van Gelderen P, de Zwart JA, Horovitz SG, Fukunaga M, Jansma JM, Duyn JH. Low-frequency fluctuations in the cardiac rate as a source of variance in the resting-state fMRI BOLD signal. Neuroimage 2007;38:306–320. [PubMed: 17869543]

Silva AC, Zhang W, Williams DS, Koretsky AP. Multi-slice MRI of rat brain perfusion during amphetamine stimulation using arterial spin labeling. Magn Reson Med 1995;33:209–214. [PubMed: 7707911]

St Lawrence KS, Frank JA, Bandettini PA, Ye FQ. Noise reduction in multi-slice arterial spin tagging imaging. Magn Reson Med 2005;53:735–738. [PubMed: 15723412]

Talagala, SL.; Chuang, KH.; Chesnick, S.; van Gelderen, P.; Koretsky, AP.; Duyn, JH. High sensitivity CASL perfusion MRI at 3T using a 16 channel receiver coil array. Proc 12th Annual Meeting ISMRM; Kyoto, Japan. 2004a. p. 717

Talagala, SL.; Slavin, GS.; Ostuni, J.; Chesnick, S. CASL perfusion MRI with non-segmented low flip angle 3D EPI. Proc 14th Annual Meeting ISMRM; Seattle, WA. 2006. p. 3422

NIH-PA Author Manuscript

NIH-PA Author Manuscript

NIH-PA Author Manuscript

Talagala SL, Ye FQ, Ledden PJ, Chesnick S. Whole-brain 3D perfusion MRI at 3.0 T using CASL with a separate labeling coil. Magn Reson Med 2004b;52:131–140. [PubMed: 15236376]

van Gelderen P, Wu WH, de Zwart JA, Cohen L, Hallett M, Duyn JH. Resolution and reproducibility of BOLD and perfusion functional MRI at 3.0 Tesla. Magn Reson Med 2005;54:569–576. [PubMed: 16086372]

Wang Z, Wang J, Connick TJ, Wetmore GS, Detre JA. Continuous ASL (CASL) perfusion MRI with an array coil and parallel imaging at 3T. Magn Reson Med 2005;54:732–737. [PubMed: 16086314]

Xiong J, Parsons LM, Gao JH, Fox PT. Interregional connectivity to primary motor cortex revealed using MRI resting state images. Hum Brain Mapp 1999;8:151–156. [PubMed: 10524607]

Ye FQ, Frank JA, Weinberger DR, McLaughlin AC. Noise reduction in 3D perfusion imaging by attenuating the static signal in arterial spin tagging (ASSIST). Magn Reson Med 2000;44:92–100. [PubMed: 10893526]

Ye FQ, Mattay VS, Jezzard P, Frank JA, Weinberger DR, McLaughlin AC. Correction for vascular artifacts in cerebral blood flow values measured by using arterial spin tagging techniques. Magn Reson Med 1997;37:226–235. [PubMed: 9001147]

Young JP, Geyer S, Grefkes C, Amunts K, Morosan P, Zilles K, Roland PE. Regional cerebral blood flow correlations of somatosensory areas 3a, 3b, 1, and 2 in humans during rest: a PET and cytoarchitectural study. Hum Brain Mapp 2003;19:183–196. [PubMed: 12811734]

Zaharchuk G, Ledden PJ, Kwong KK, Reese TG, Rosen BR, Wald LL. Multislice perfusion and perfusion territory imaging in humans with separate label and image coils. Magn Reson Med 1999;41:1093–1098. [PubMed: 10371440]

NIH-PA Author Manuscript
NIH-PA Author Manuscript
NIH-PA Author Manuscript

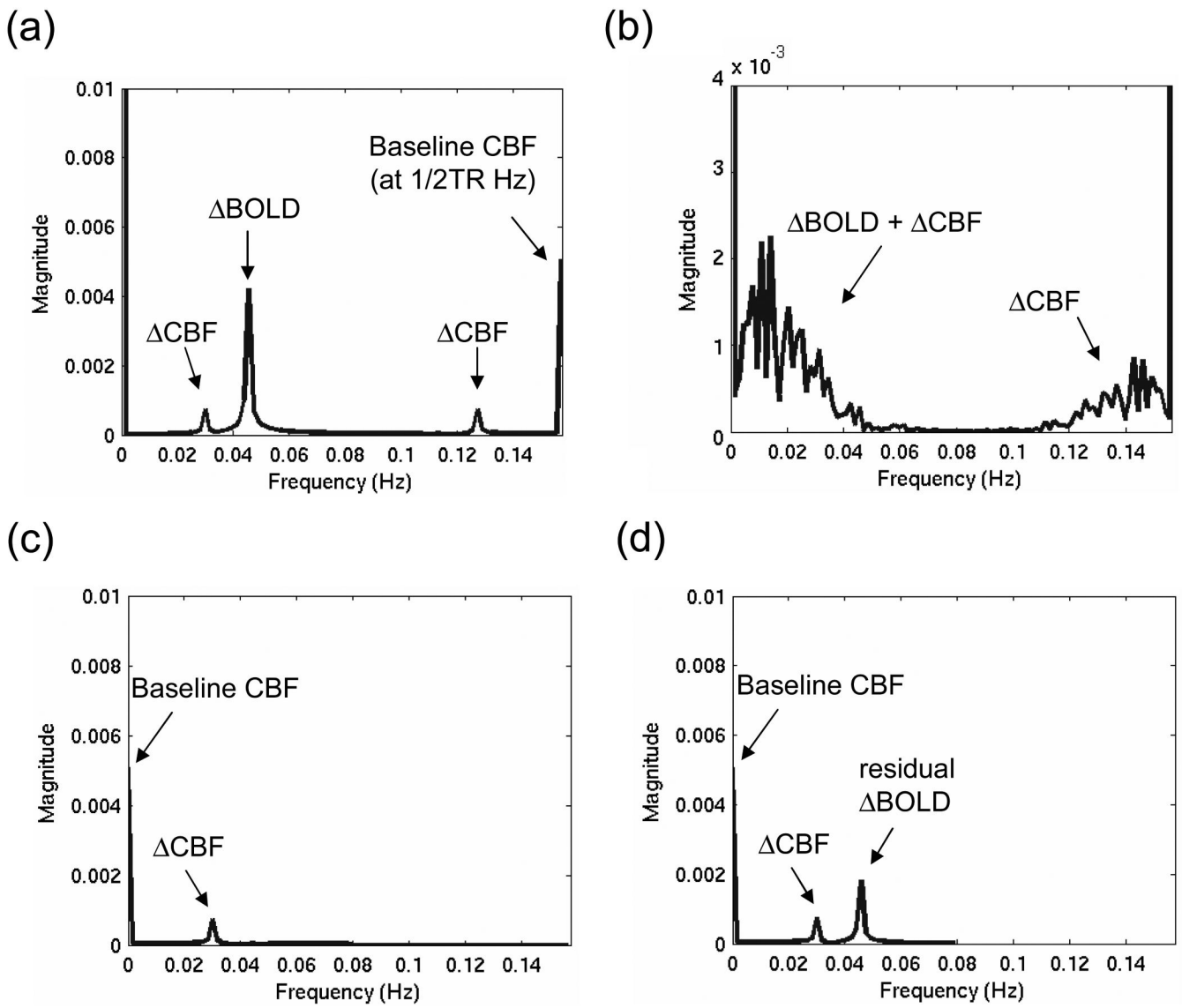

Fig. 1.

Magnitude spectra of simulated ASL signals assuming (a) CBF fluctuation (ΔCBF) at 0.03 Hz and BOLD fluctuation (ΔBOLD) at 0.045 Hz, (b) ΔCBF and ΔBOLD both at multiple frequencies with bandwidths < 0.08 Hz. The CBF and BOLD oscillations can be seen in low frequency range while only CBF fluctuations exist in high frequency range. The magnitude spectra of the signal in (a) processed by (c) the proposed high-pass filtering and demodulation method and (d) pair-wise subtraction and low-pass filtering at 0.064 Hz. The 0.064 Hz cutoff frequency was chosen to maintain the same sampling bandwidth to filter cutoff ratio used previously (Biswal et al., 1997). It can be seen that significant BOLD signal remained when using pair-wise subtraction and low-pass filtering. In this simulation, the magnitudes of CBF and BOLD fluctuations were assumed as 30% and 0.9%, respectively, with 1% signal change due to labeling and TR = 3.2 s.

NIH-PA Author Manuscript
NIH-PA Author Manuscript
NIH-PA Author Manuscript

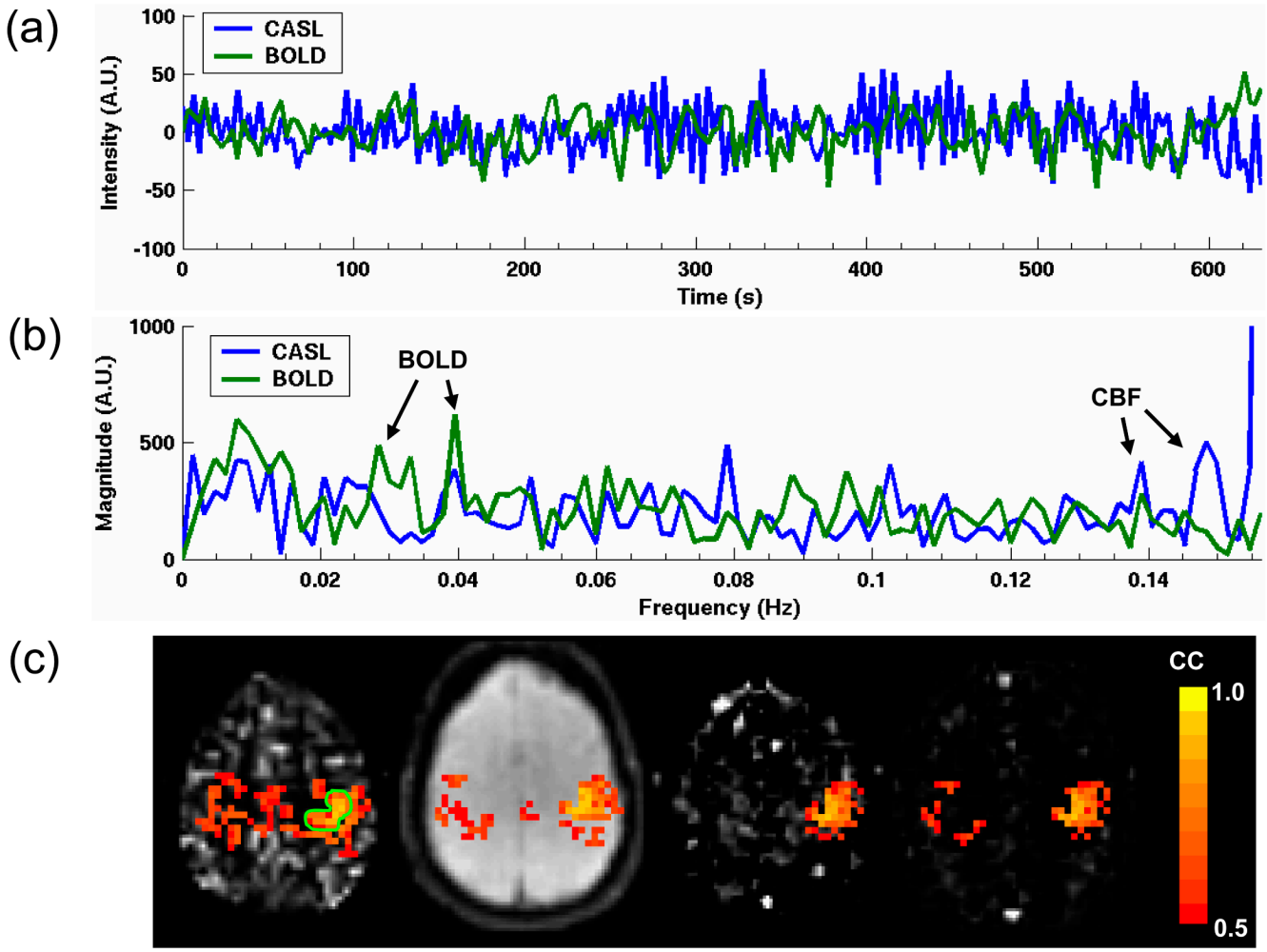

Fig. 2.

The (a) time courses and (b) spectra of unfiltered resting-state CASL and BOLD data from an ROI in the left motor area (the green region in c). (c) Correlation maps showing functional connectivity obtained using high-pass CASL data (left; high-pass filter cutoff 0.08 Hz), standard BOLD data (2nd from the left; high-pass filter cutoff 0.003 Hz), high-pass BOLD data (3rd from the left; filter cutoff 0.08 Hz), and pair-wise subtracted (with low-pass filter at 0.064 Hz) BOLD data (right). Except for standard BOLD, the thresholded statistical maps are overlaid on the average image after filtering or subtraction. The thresholded map for standard BOLD is overlaid on averaged raw image without filtering. High correlation can be observed between bilateral sensorimotor areas in the high-pass CASL data and standard BOLD data. The presence of bilateral correlation in the pair-wise subtracted BOLD data, but not in the high-pass BOLD data, indicates the effectiveness of high-pass filtering in suppressing BOLD fluctuations in CBF-based connectivity maps.

NIH-PA Author Manuscript

NIH-PA Author Manuscript

NIH-PA Author Manuscript

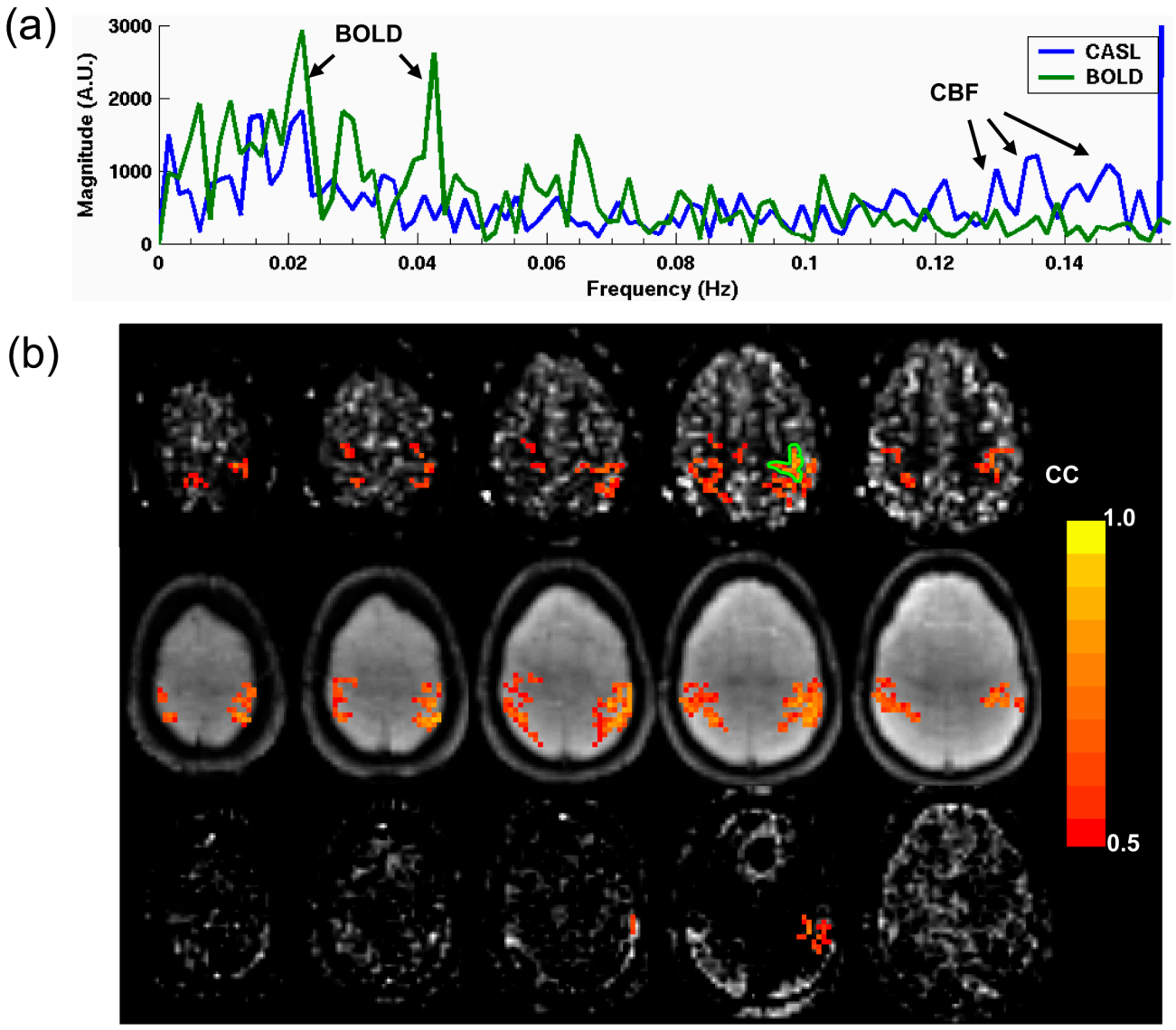

Fig. 3.

(a) Unfiltered resting state CASL and BOLD spectra from the motor ROI (indicated in (b)) shows well separated BOLD (< 0.08 Hz) and CBF (> 0.08 Hz) fluctuations in frequency domain. (b) Multi-slice functional connectivity maps obtained with high-pass CASL (top), standard BOLD (middle), and high-pass BOLD (bottom) data using a motor ROI (the green region) time course for correlation. High correlation can be found between bilateral sensorimotor areas across several slices in the high-pass CASL and standard BOLD data, but not in the high-pass BOLD data.

NIH-PA Author Manuscript

NIH-PA Author Manuscript

NIH-PA Author Manuscript

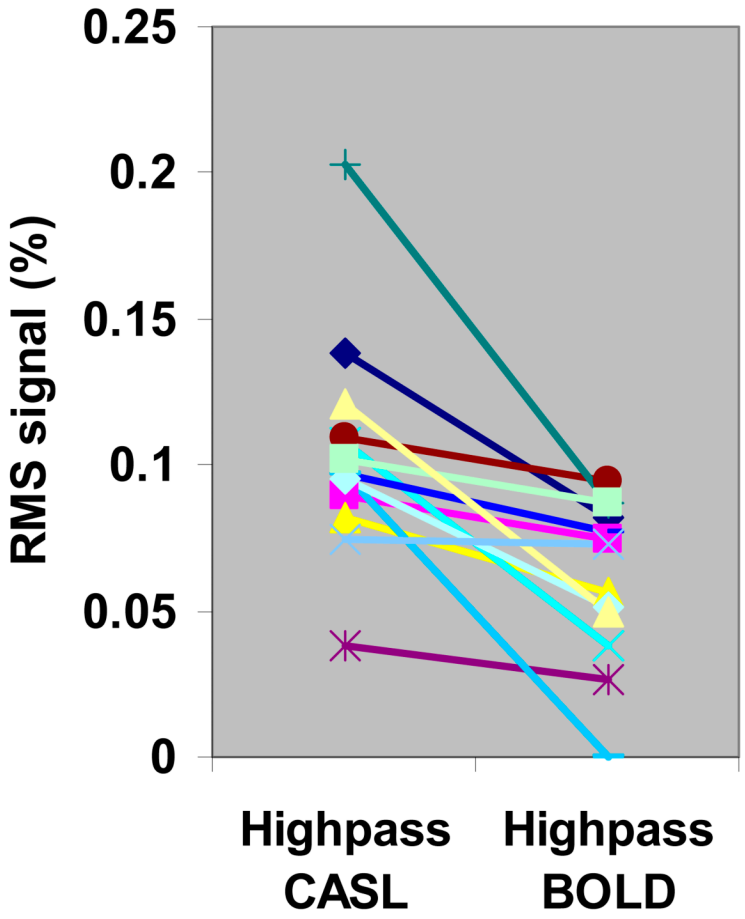

Fig. 4.

Percent RMS amplitudes of selected frequencies in the motor ROIs in high-pass CASL and high-pass BOLD data for 13 subjects. The frequencies were selected by applying an cc_f threshold (between 0.01 – 0.02) to the CC spectrum. RMS signal in high-pass CASL is significantly higher ($p < 0.001$, two-tail paired t-test) than high-pass BOLD data.

NIH-PA Author Manuscript

NIH-PA Author Manuscript

NIH-PA Author Manuscript

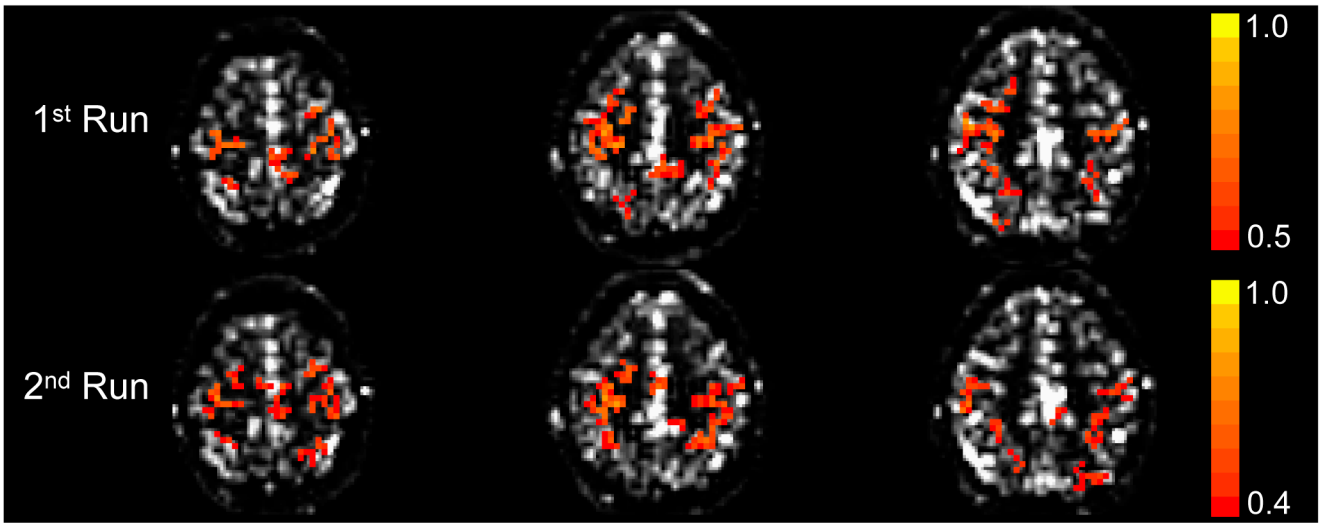

Fig. 5.

Separate acquisitions of CBF-based functional connectivity maps obtained within the same session. Three adjacent slices from each run are shown. The maps were highly reproducible (similarity index of unthresholded maps = 0.88) across different runs. A lower CC threshold was used to display the functionally connected regions in the second run.

NIH-PA Author Manuscript

NIH-PA Author Manuscript

NIH-PA Author Manuscript

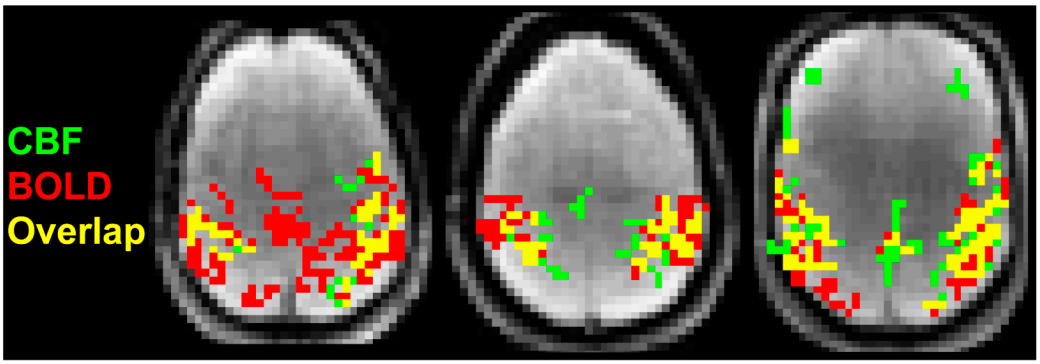

Fig. 6.

Composite functional connectivity maps showing BOLD (red), CBF (green), and the BOLD/CBF overlap (yellow) areas in 3 subjects (from left to right). The CC threshold was the same for all data within each subject, but different among subjects (from left to right CC = 0.47, 0.5, and 0.6).

NIH-PA Author Manuscript NIH-PA Author Manuscript NIH-PA Author Manuscript

Table 1

The percent RMS amplitudes and peak frequencies of CBF and BOLD fluctuations in the reference ROIs. The RMS amplitudes were calculated from frequencies contributing to the bilateral sensorimotor connectivity (CBF_{cor} and $BOLD_{cor}$) and from all frequencies (CBF_{total} and $BOLD_{total}$). The signal changes are relative to the baseline CBF or the mean image intensity (BOLD). The peak frequencies (CBF_{peak} and $BOLD_{peak}$) were determined from the CC spectra.

Subject	CBF_{cor} (%)	CBF_{total} (%)	$BOLD_{cor}$ (%)	$BOLD_{total}$ (%)	CBF_{peak} (Hz)	$BOLD_{peak}$ (Hz)
1	33	42	0.56	0.65	0.013	0.016
2	71	149	0.20	0.32	0.014	0.023
3	60	106	0.25	0.30	0.045	0.030
4	36	56	0.16	0.27	0.046	0.015
5	5.8	26	0.08	0.20	0.072	0.025
6	8.9	30	0.10	0.22	0.033	0.023
7	35	42	0.48	0.52	0.020	0.022
8	24	51	0.36	0.42	0.019	0.013
9	34	41	0.25	0.28	0.017	0.016
10	25	42	0.23	0.26	0.008	0.019
11	12	21	0.13	0.25	0.019	0.0047
12	17	23	0.29	0.34	0.021	0.0016
13	15	31	0.30	0.42	0.011	0.019
Mean ± STD	29 ± 19	51 ± 37	0.26 ± 0.14	0.34 ± 0.13	0.026 ± 0.018	0.017 ± 0.008